Spectral-Encoded UWB Communication Systems: Real-Time Implementation and Interference Suppression

Claudio R. C. M. da Silva, *Student Member, IEEE,* and Laurence B. Milstein, *Fellow, IEEE*

***Abstract*—This paper considers a particular implementation of an ultra-wideband communication system that uses spectral encoding as both the multiple-access scheme and the interference-suppression technique. The main advantage of this technique is that the transmitted signal spectrum can be conveniently shaped to suppress narrowband interference and to not cause noticeable interference to overlaid systems. An extensive analysis of a possible implementation of this system by using surface acoustic-wave models is presented, and general expressions for the system performance are obtained. Numerical results show that a significant improvement in the system performance is obtained when the proposed interference-suppression method is used.**

***Index Terms*—Narrowband interference (NBI) suppression, spectral encoding, surface acoustic wave (SAW) devices, ultra-wideband (UWB).**

I. Introduction

AIMING for more efficient spectrum use, the FCC allocated in early 2002 a 7.5-GHz bandwidth for ultra-wideband (UWB) communication systems that, as opposed to conventional systems, forces its coexistence with narrowband systems [1]. This spectrum allocation is a significant breakthrough from traditional exclusive-based allocation policies that have been the norm since the genesis of wireless communication systems, and is one of the main reasons for the high interest of both academic and industry groups in UWB systems [2]. Spectral overlay is possible, at least in principle, due to the negligible level of interference that very low power spectral density (PSD) UWB signals would cause to overlaid narrowband systems.

The low PSD is only one of the many desirable characteristics of UWB signals. UWB communication systems were originally based upon impulse-radio technology[1] [3]–[5]. In this technology, baseband pulses of very short time duration, typically on the order of a nanosecond, are transmitted. This is very attractive for both communication and positioning systems because of its low cost of implementation, since it is a *carrierless* radio, and lack of significant fading [6], [7], due to its fine multipath resolution. However, when UWB transitioned from a research topic to actual consideration for commercial communications applications, the technologies of choice for UWB systems were more conventional carrier-based transmission schemes, rather than the impulse radio [8]. The main reason for this shift is that the power mask defined by the FCC limits the UWB transmission to the 3.1–10.6 GHz region, forcing (baseband) impulse-radio devices to employ some sort of additional transmit filtering [9]. For example, the IEEE 802.15.3 standardization group, which began by considering different modulation formats, including impulse radio, narrowed down its choices to either code-division multiple access (CDMA) [10] or orthogonal frequency-division multiplexing (OFDM) [11] technologies. Some examples of recent trends in UWB communication systems can be found in [12], and a UWB network study can be found in [13].

Independent of the transmission technique used, an important concern in UWB system design is the minimization of the possible interference to and from narrowband systems that are overlaid by UWB signals. Different techniques have been proposed to overcome this problem; for example, minimum mean-square error (MMSE)-based receivers were considered in [14] and [15] for impulse-radio-based systems, and an OFDM system was proposed in [16]. In this paper, we consider an alternative, *carrier*-based, modulation scheme for UWB systems based on the spectral-encoded technology. In this system, spectral encoding is used as both the multiple-access scheme and the narrowband interference (NBI)-suppression method. The main contributions of this paper are: 1) the extension of spectral-encoded systems to a UWB environment with a RAKE configuration; 2) analysis of a possible real-time implementation of spectral-encoded systems with the use of surface acoustic devices; and 3) performance analysis in the presence of NBI with and without interference suppression.

The remaining parts of this paper are organized as follows. The spectral-encoded concept is introduced in Section II. A real-time implementation of the transmitter and receiver are presented and analyzed in Sections III and IV, respectively. A formulation of the noise and interference components is presented in Section V. In Section VI, numerical results of the system performance are presented, and conclusions are drawn in Section VII.

Paper approved by M. Z. Win, the Editor for Equalization and Diversity of the IEEE Communications Society. Manuscript received August 29, 2003; revised November 23, 2004. This work was supported in part by the Center for Wireless Communications at UCSD, in part by the UC Discovery Program of the State of California, and in part by the National Science Foundation under Grant NSF-0123405. This paper was presented in part at the 2003 IEEE Conference on Ultra-Wideband Systems and Technologies, Reston, VA, November 2003.

The authors are with the Department of Electrical and Computer Engineering, University of California, San Diego, CA 92093-0407 USA (e-mail: claudio.silva@ieee.org; milstein@ece.ucsd.edu).

Digital Object Identifier 10.1109/TCOMM.2005.852822

[1]There is some confusion in the literature between the definitions of *UWB* and *impulse radio*. The FCC defines UWB as *any* wireless transmission technique that occupies more than 500 MHz of absolute bandwidth, or 20% of its center frequency [1]. Impulse radio, together with technologies such as code-division multiple access and orthogonal frequency-division multiplexing, are possible technologies for implementing UWB systems.

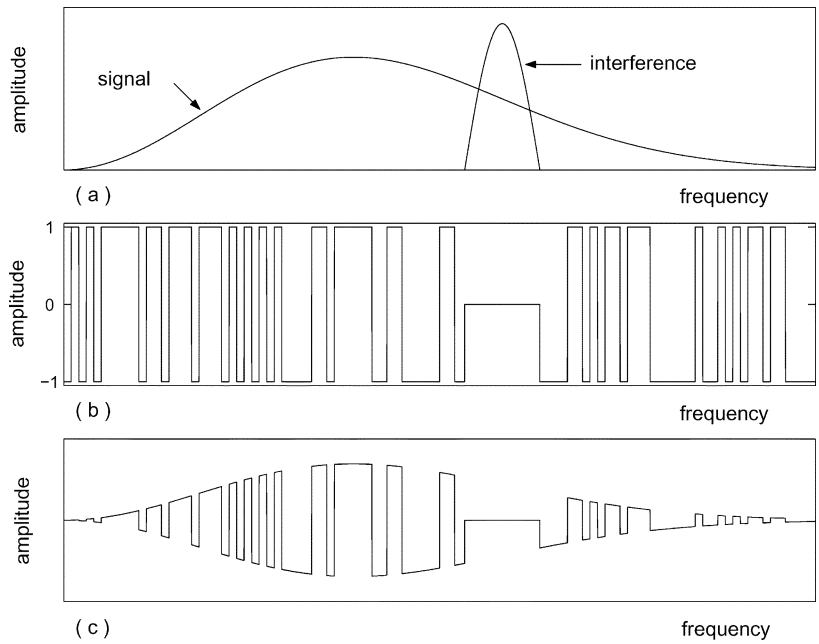

Fig. 1. Graphical representation of the encoding process and interference suppression. (a) Spectrum of the conventional signal and interference. (b) Spectral binary (± 1) encoding sequence. (c) Spectrum of the transmitted signal.

II. Spectral-Encoded UWB Communication Systems

The spectral-encoding concept was first proposed in an optical-communication context [17], [18], and was then extended to a wireless-communications scenario in [19] and [20]. In this technique, a conventional signal is multiplied by a spreading sequence in the frequency domain. As a result, the signal spreads in time. Consequently, the spectral-encoding technique can be considered as the frequency-domain counterpart to a conventional direct-sequence (DS)/CDMA spread-spectrum system. Multiple-access capability is achieved by assigning distinct spreading sequences to different users.

In this paper, we extend the spectral-encoding concept to also achieve NBI suppression via the spectral encoding. When interference suppression[2] is desired, a spreading sequence is used which has a spectral null where the NBI is located. A graphical representation of the encoding process and interference suppression is shown in Fig. 1. It can be seen in this figure that the transmitted spectral encoded signal does not have spectral components over a range of frequencies where the NBI is the strongest. In addition, the NBI is "notched out" at the receiver when the received signal spectrum is multiplied by the conjugate of the transmitted signal spectrum (despreading operation).

Although spectral-encoded systems have a greater implementation complexity than conventional techniques, this system does not need additional circuitry to perform spectral-shaping/NBI suppression. In contrast, UWB systems based on either impulse radio or CDMA transmission techniques, for example, may need to employ notch filters or MMSE receivers to diminish the spectral overlay effects.

[2]The idea of considering spectral-encoded systems in a UWB scenario to achieve NBI suppression was presented by the authors at the "An Ultra-Wideband Technology Workshop: From Research to Reality," held at the University of Southern California, Los Angeles, October 2002.

More recently [21], [22], Shayesteh *et al.* extended the analysis presented in [19] and [20] to consider fading channels. It is pointed out in [22] that the spectral-encoding technique can be advantageous for UWB systems, because the spreading in time resulting from the encoding process reduces the effective instantaneous power of the transmitted signal. Based on a detailed analysis of the multiple-access interference, general expressions for the signal-to-interference-plus-noise ratio (SIR) for both spectral-encoded CDMA and DS/CDMA are derived in [19]–[22]. It is shown that, in the absence of thermal noise, the performance of the spectral-encoded CDMA system is equal to or better than that of a DS/CDMA system. It is important to note that the system to be considered in this paper is a particular case of the systems described in [19]–[22]. As opposed to [19]–[22], this paper is interested with the performance analysis, in terms of bit-error rate (BER), of spectral-encoded systems in the presence of NBI and its implementation using real-time devices.

III. Transmitter Design

A schematic of the transmitter can be found in Fig. 2. The transmitter consists of the following stages: generation of a conventional waveform, modulation, real-time Fourier transformation, multiplication by a spreading sequence, real-time inverse Fourier transformation, and lowpass filtering. The real-time Fourier-transform stages are based upon the use of surface acoustic wave (SAW) devices, and correspond to the models proposed in [23]. Specifically, the Fourier transform is based on a well-established implementation (see, e.g., [23, refs. [1]–[4]]), which corresponds to the multiplication and convolution of the desired signal by chirp (linear FM) waveforms. SAW devices have evolved to the GHz range and "currently, submicron manufacturing and material techniques are improving greatly and encompassing even higher frequencies of up to 10

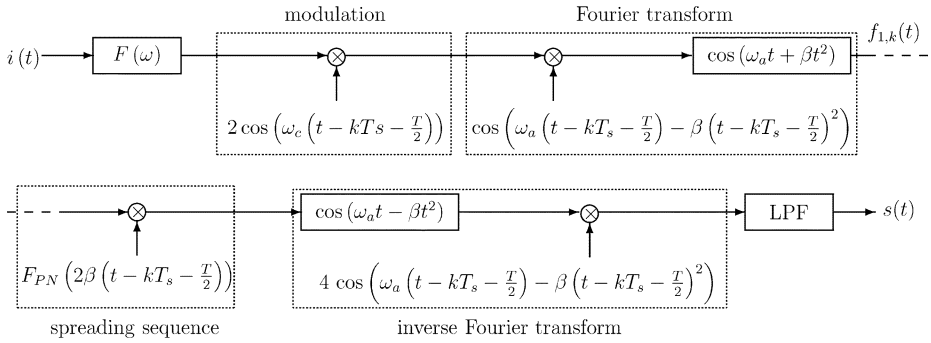

Fig. 2. Transmitter model using SAW devices.

GHz" [24]. In addition, "(SAW devices) can perform real-time correlation of signals with absolute bandwidths up to a few hundred MHz easily" [25].

In Fig. 2, the function $i(t)$ is defined as

$$i(t)=\sum_{k=-\infty}^{\infty} d[k]\,\delta\left(t-kT_s-\frac{T}{2}\right) \tag{1}$$

where $d[k]$ is the data to be transmitted, composed of a ± 1 sequence with period T_s. The conventional waveform $f(t)$, generated by the impulse response of the filter $F(w)$, is assumed to be nonzero only in $t\in[-T/2,T/2]$. To ignore intersymbol interference, we assume $T_s>T+T_m$, where T_m is the multipath spread. Let us consider, without loss of generality, the receiver during the transmission of the nth symbol. In this case, as can be seen in Fig. 2, the output of the Fourier-transform stage, denoted by $f_{1,n}(t)$, is given by

$$\begin{aligned} f_{1,n}(t)=2d[n]\int_{nT_s}^{nT_s+T} & f\left(\tau-nT_s-\frac{T}{2}\right)\cos\left(\omega_c\left(\tau-nT_s-\frac{T}{2}\right)\right)\\ &\times\cos\left(\omega_a\left(\tau-nT_s-\frac{T}{2}\right)-\beta\left(\tau-nT_s-\frac{T}{2}\right)^2\right)\\ &\times\cos\left(\omega_a(t-\tau)+\beta(t-\tau)^2\right)d\tau \end{aligned} \tag{2}$$

where the parameters ω_a and β are, respectively, the center frequency and half-slope of the chirp signals, and ω_c is the carrier frequency. Simplifying, $f_{1,n}(t)$ yields

$$\begin{aligned} f_{1,n}(t)=&\frac{1}{2}F_R\left(2\beta\left(t-nT_s-\frac{T}{2}\right)\right)\\ &\times\cos\left(\omega_a\left(t-nT_s-\frac{T}{2}\right)+\beta\left(t-nT_s-\frac{T}{2}\right)^2\right)\\ &-\frac{1}{2}F_I\left(2\beta\left(t-nT_s-\frac{T}{2}\right)\right)\\ &\times\sin\left(\omega_a\left(t-nT_s-\frac{T}{2}\right)+\beta\left(t-nT_s-\frac{T}{2}\right)^2\right) \end{aligned} \tag{3}$$

where a double-frequency term has been ignored. The functions $F_R(2\beta(t-nT_s-T/2))$ and $F_I(2\beta(t-nT_s-T/2))$ are, respectively, the real and imaginary components of the Fourier transform of the modulated $f(t)$, i.e., they are given by

$$\begin{aligned} &F_R\left(2\beta\left(t-nT_s-\frac{T}{2}\right)\right)\\ &\quad=2d[n]\int_{-\frac{T}{2}}^{\frac{T}{2}} f(\xi)\cos(\omega_c\xi)\\ &\qquad\times\cos\left(2\beta\left(t-nT_s-\frac{T}{2}\right)\xi\right)d\xi \end{aligned} \tag{4}$$

$$\begin{aligned} &F_I\left(2\beta\left(t-nT_s-\frac{T}{2}\right)\right)\\ &\quad=-2d[n]\int_{-\frac{T}{2}}^{\frac{T}{2}} f(\xi)\cos(\omega_c\xi)\\ &\qquad\times\sin\left(2\beta\left(t-nT_s-\frac{T}{2}\right)\xi\right)d\xi. \end{aligned} \tag{5}$$

Note from (4) and (5) that the angular frequency evolves in real time according to $\omega=2\beta(t-nT_s-T/2)$. We assume, for simplicity of presentation, that the real signal $f(t)$ is even. Therefore, $F_I(\cdot)$, given by (5), is equal to zero.

The Fourier transform of $f(t)$, given by (3), is only valid during the interval of time that $f(t)$ is fully contained in the filter labeled $\cos(\omega_a t+\beta t^2)$ in Fig. 2. Assuming that the impulse response of this filter is T_1 s long, with $T<T_1$, $f_{1,n}(t)$ is only valid in $t\in[nT_s+T,nT_s+T_1]$. In the same way, the inverse Fourier transform is only valid when its input is fully contained in the filter labeled $\cos(\omega_a t-\beta t^2)$. Therefore, the encoded symbol also has duration T, and the nth symbol is only valid in $t\in[nT_s+T_1,nT_s+T_1+T]$. As a consequence, the output of the transmitter is, in fact, a time-truncated version of the desired signal. As previously observed, the multiplication by a spreading sequence in the frequency domain leads to a spreading in the time domain; therefore, T must be large enough to contain most of the spread signal energy. It is shown in Section IV that $f(t)$ is a lowpass signal with bandwidth W Hz, thus it has infinite duration. Since T is assumed to contain most of the spread signal energy, it is reasonable to disregard the time-truncation effects in $f_{1,n}(t)$. However, the time truncation in the transmitted signal cannot be ignored, and the system performance is a function of this truncation.

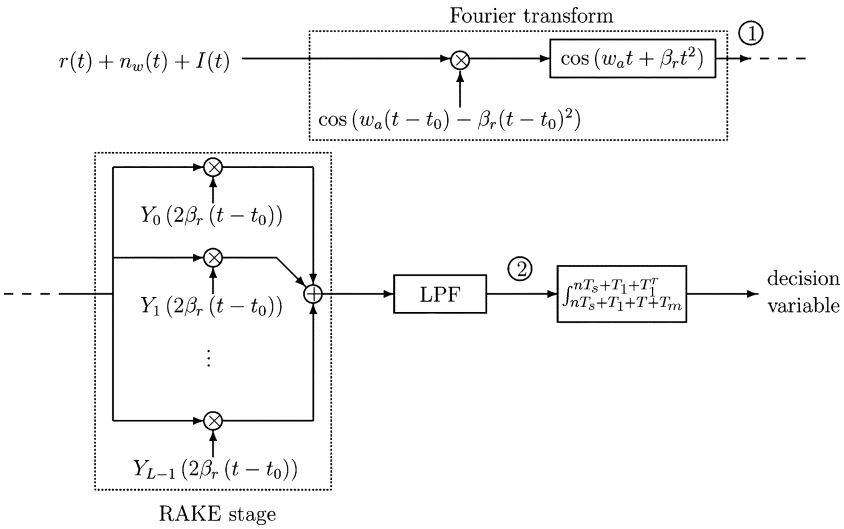

Fig. 3. Receiver model using SAW devices.

As $\omega = 2\beta(t-nT_s-T/2)$, and since $f_{1,n}(t)$ is only valid for $t \in [nT_s+T, nT_s+T_1]$, the range over which (3) yields a true Fourier transform is $\omega \in [2\beta T/2, 2\beta(T_1-T/2)]$. Therefore, β and T_1 must be chosen such that $2\beta T/2 = \omega_c - \pi W$ and $2\beta(T_1-T/2) = \omega_c + \pi W$.

It is desired to multiply $f_{1,n}(t)$ by a spreading sequence given by $PN(\omega) = PN_R(\omega) + jPN_I(\omega)$, where $PN(\omega)$ is, in general, a complex waveform, bandlimited to $|f| \le W/2$. $PN_R(\omega)$ and $PN_I(\omega)$ consist of a sequence of ± 1's (and zeros, when interference suppression is considered). The function $F_{PN}(2\beta(t-nT_s-T/2))$ in Fig. 2 is related to $PN(\omega)$ by

$$\begin{aligned} F_{PN}&\left(2\beta\left(t-nT_s-\frac{T}{2}\right)\right) \\ &= \frac{8\beta}{\pi}\left[PN_R\left(2\beta\left(t-nT_s-\frac{T}{2}\right)\right)\right. \\ &\qquad \times \cos\left(2\beta\left(t-nT_s-\frac{T}{2}\right)T_1\right) \\ &\qquad + PN_I\left(2\beta\left(t-nT_s-\frac{T}{2}\right)\right) \\ &\qquad \left. \times \sin\left(2\beta\left(t-nT_s-\frac{T}{2}\right)T_1\right)\right]. \end{aligned} \tag{6}$$

By using an analysis similar to the one developed for the forward Fourier transformation, the transmitted signal $s_n(t)$ corresponding to the nth symbol can be written as

$$\begin{aligned} s_n(t) = \frac{d[n]}{\pi}\int_{\omega_c-\pi W}^{\omega_c+\pi W}&\left[R(\omega)\cos\left(\omega\left(t-nT_s-\frac{T}{2}-T_1\right)\right)\right. \\ &\left. -I(\omega)\sin\left(\omega\left(t-nT_s-\frac{T}{2}-T_1\right)\right)\right]d\omega. \end{aligned} \tag{7}$$

In (7), $\omega = 2\beta(\tau - nT_s - T/2)$, and $R(\omega)$ and $I(\omega)$ are defined as

$$R(\omega) = F_R(\omega)PN_R(\omega) \quad \text{and} \quad I(\omega) = F_R(\omega)PN_I(\omega) \tag{8}$$

i.e., $R(\omega)$ and $I(\omega)$ correspond, respectively, to the real and imaginary parts of the transmitted signal. It is important to recall that $s_n(t)$ is valid only in $t \in [nT_s+T_1, nT_s+T_1+T]$.

IV. Receiver Design

It is assumed that the transmitted signal passes through a frequency-selective fading channel with (lowpass-equivalent) impulse response given by

$$h(t) = \sum_{l=0}^{L-1} \alpha_l(t)e^{-j\phi_l(t)}\delta(t-\tau_l) \tag{9}$$

where L is the number of resolvable paths, and $\alpha_l(t)$ and $\phi_l(t)$ are, respectively, the amplitude and phase of the lth multipath component.[3] The phases $\phi_l(t)$, $l = 0, \ldots, L-1$, are assumed to be independent and uniformly distributed in $[0, 2\pi)$. The channel is assumed to be slowly varying, thus the time dependency in $\alpha_l(t)e^{-j\theta_l(t)}$ is dropped. Since the band occupancy of the complex envelope of the transmitted signal considered in this paper is equal to $|f| \le W/2$, it is assumed that a resolution equal to $1/W$ is achieved in the multipath delay profile [29]. Therefore, $\tau_l = l/W$. Assume, without loss of generality, the detection of the nth symbol. Also, assume $d[n] = 1$. By using (7) and (9), the received signal $r(t)$ is given by

$$\begin{aligned} r(t) = \sum_{l=0}^{L-1}\alpha_l\frac{1}{\pi}\int_{\omega_c-\pi W}^{\omega_c+\pi W}&\left[R(\omega)\cos\left(\omega\left(t-nT_s-\frac{T}{2}-T_1-\tau_l\right)-\phi_l\right)\right. \\ &\left. -I(\omega)\sin\left(\omega\left(t-nT_s-\frac{T}{2}-T_1-\tau_l\right)-\phi_l\right)\right]d\omega. \end{aligned} \tag{10}$$

A receiver for the proposed system is shown in Fig. 3, and consists of a real-time Fourier transformation device, a RAKE stage, a lowpass filter (LPF), and an integrate-and-dump. In addition to the desired signal, it is assumed that additive thermal noise $n_w(t)$ and interference $I(t)$ are present at the receiver's input. The noise and interference are considered in Section V.

The interaction time T_1 and the half-slope β of the receiver's Fourier transform device are denoted by T_1^r and β_r, respectively.

[3]Note that the UWB channel models presented in [26] and [27] do not consider phase shifts. This is because these models assume the transmission of carrierless baseband pulses. In our case, the system has a carrier, and therefore, it makes sense to include a carrier shift. In the IEEE 802.15 channel model [28], the multipath coefficients are multiplied by an equiprobable ± 1 variable, to account for signal inversion due to reflections, which can be seen as phase variations equal to $\{0, \pi\}$.

Since the channel has a multipath spread equal to T_m, the time window that the Fourier transform device must consider is $T+T_m$ long; therefore, recalling that the transmitter's output for the nth symbol is valid only in the range $[nT_s+T_1, nT_s+T_1+T]$, the time window $[nT_s+T_1, nT_s+T_1+T+T_m]$ must be used. Ignoring temporarily the noise and interference at the receiver's input, the function $f_1^r(t)$ at point 1 in Fig. 3 is equal to

$$f_1^r(t) = \int_{nT_s+T_1}^{nT_s+T_1+T+T_m} r(\tau)\cos\left(\omega_a(\tau-t_0)-\beta_r(\tau-t_0)^2\right) \times \cos\left(\omega_a(t-\tau)+\beta_r(t-\tau)^2\right)d\tau \quad (11)$$

where t_0 is defined as $t_0 = nT_s + T_1 + T/2$, and $r(\tau)$ is given by (10). Substituting $r(t)$ in (11), $f_1^r(t)$ can be simplified to

$$\begin{aligned} f_1^r(t) \cong{}& \frac{1}{2}\cos\left(\omega_a(t-t_0)+\beta_r(t-t_0)^2\right) \\ &\times\left(\sum_{l=0}^{L-1}\alpha_l F_c\left(2\beta_r(t-t_0),l\right)\right) \\ &-\frac{1}{2}\sin\left(\omega_a(t-t_0)+\beta_r(t-t_0)^2\right) \\ &\times\left(\sum_{l=0}^{L-1}\alpha_l F_s\left(2\beta_r(t-t_0),l\right)\right) \end{aligned} \quad (12)$$

where a double-frequency component has been ignored, and $F_c(2\beta_r(t-t_0),l)$ and $F_s(2\beta_r(t-t_0),l)$ are defined as follows:

$$F_c\left(2\beta_r(t-t_0),l\right) = \int_{-\frac{T}{2}+\tau_l}^{\frac{T}{2}+\tau_l} x_l(\xi)\cos\left(2\beta_r(t-t_0)\xi\right)d\xi \quad (13)$$

$$F_s\left(2\beta_r(t-t_0),l\right) = -\int_{-\frac{T}{2}+\tau_l}^{\frac{T}{2}+\tau_l} x_l(\xi)\sin\left(2\beta_r(t-t_0)\xi\right)d\xi \quad (14)$$

and $x_l(\xi)$ is defined as

$$x_l(\xi) = \frac{1}{\pi}\int_{\omega_c-\pi W}^{\omega_c+\pi W} R(\omega)\cos\left(\omega(\xi-\tau_l)-\phi_l\right) - I(\omega)\sin\left(\omega(\xi-\tau_l)-\phi_l\right)d\omega. \quad (15)$$

Note that (13) and (14) correspond, respectively, to the real and imaginary components of the time-truncated Fourier transform of the lth multipath component of the received signal. It is important to note from (13) and (14) that the angular frequency now evolves in time according to $\omega = 2\beta_r(t-t_0)$.

The function $Y_k(2\beta_r(t-t_0))$, $k=0,\ldots,L-1$ in the RAKE stage is given by

$$\begin{aligned} Y_k\left(2\beta_r(t-t_0)\right) = {}& \frac{8\beta_r}{\pi}\cos\left(\omega_a(t-t_0)+\beta_r(t-t_0)^2\right) \\ &\times g_k\Lambda_c\left(2\beta_r(t-t_0),k\right) \\ &-\frac{8\beta_r}{\pi}\sin\left(\omega_a(t-t_0)+\beta_r(t-t_0)^2\right) \\ &\times g_k\Lambda_s\left(2\beta_r(t-t_0),k\right) \end{aligned} \quad (16)$$

where the following functions were defined:

$$\Lambda_c(\omega,k) = R(\omega)\cos(\omega\tau_k+\phi_k) + I(\omega)\sin(\omega\tau_k+\phi_k) \quad (17)$$

$$\Lambda_s(\omega,k) = I(\omega)\cos(\omega\tau_k+\phi_k) - R(\omega)\sin(\omega\tau_k+\phi_k). \quad (18)$$

In (17) and (18), the relation $\omega = 2\beta_r(t-t_0)$ is used, and the functions $R(\omega)$ and $I(\omega)$ are given by (8).

As the number of multipath components is high, the channel-estimation process necessary in maximal ratio combining (MRC) can be burdensome. For example, it is shown in [7] and [30] that it might be necessary to combine approximately 50 multipath components to achieve a good tradeoff between energy capture and diversity in dense multipath environments. As a consequence, we also consider suboptimum schemes, like equal gain combining (EGC), as well as generalized selection-combining techniques [31], whereby the latter schemes are based upon MRC and EGC (denoted by SC/MRC and SC/EGC, respectively). The analysis presented here corresponds to the MRC technique, and can be extended to the suboptimum schemes. It is important to note that in the EGC case, the gains g_k in (16) would be unitary (no amplitude estimation is performed), and in the generalized schemes, the gains corresponding to multipath components with small absolute values are set to zero. As shown in this paper, when nonideal time-truncated Fourier transforms are considered, there is self-interference between the multipath components, and the noise components in the "RAKE fingers" are correlated. This fact, together with the presence of NBI, implies that MRC in this case is not the optimum maximum-likelihood (ML) detector. However, it can be shown that the system performance when NBI is suppressed by using spectral encoding closely approximates that of an optimum ML detector [32].

The function $f_2^r(t)$ at point 2 in Fig. 3 is given by

$$\begin{aligned} f_2^r(t) = {}& \frac{2\beta_r}{\pi}\left[\sum_{l=0}^{L-1}\alpha_l F_c\left(2\beta_r(t-t_0),l\right)\right] \\ &\times\left[\sum_{k=0}^{L-1} g_k\Lambda_c\left(2\beta_r(t-t_0),k\right)\right] \\ &+\frac{2\beta_r}{\pi}\left[\sum_{l=0}^{L-1}\alpha_l F_s\left(2\beta_r(t-t_0),l\right)\right] \\ &\times\left[\sum_{k=0}^{L-1} g_k\Lambda_s\left(2\beta_r(t-t_0),k\right)\right] \end{aligned} \quad (19)$$

where it is assumed that double-frequency terms of the form $2\omega_a(t-t_0)+2\beta_r(t-t_0)^2$ are filtered out by the LPF. The decision variable is obtained by integrating the sum of all the RAKE finger outputs. Letting $\omega = 2\beta_r(t-t_0)$, the information component of the decision variable is given by

$$\Delta = \frac{1}{\pi}\sum_{l=0}^{L-1}\sum_{k=0}^{L-1}\alpha_l g_k \int_{\omega_c-\pi W}^{\omega_c+\pi W} (F_c(\omega,l)\Lambda_c(\omega,k) + F_s(\omega,l)\Lambda_s(\omega,k))\,d\omega. \quad (20)$$

Consider now the effects of the truncation in time. We first consider a theoretical system where the Fourier transforms are not time-truncated (which corresponds to $T \to \infty$), and then consider the real-time implementation (T assuming a finite value).

A. Ideal Fourier Transform Device

The *non*-time-truncated versions of $F_c(\omega, n)$ and $F_s(\omega, n)$ are obtained by letting $T \to \infty$ in the integral limits of (13) and (14), respectively. In this case, we obtain

$$F_c(\omega, l) = R(\omega)\cos(\omega\tau_l + \phi_l) + I(\omega)\sin(\omega\tau_l + \phi_l) \quad (21)$$

$$F_s(\omega, l) = I(\omega)\cos(\omega\tau_l + \phi_l) - R(\omega)\sin(\omega\tau_l + \phi_l). \quad (22)$$

It should be noticed that $F_c(\omega, l)$ and $F_s(\omega, l)$ are valid only for $\omega_c - \pi W \le \omega \le \omega_c + \pi W$. The decision variable is obtained by substituting the functions $F_c(\omega, l)$, $F_s(\omega, l)$, $\Lambda_c(\omega, k)$, and $\Lambda_s(\omega, k)$ given, respectively, by (21), (22), (17), and (18), in (20). The result is

$$\Delta = \frac{1}{\pi}\sum_{l=0}^{L-1}\sum_{k=0}^{L-1}\alpha_l g_k \int_{\omega_c-\pi W}^{\omega_c+\pi W}\left(R^2(\omega) + I^2(\omega)\right) \times \cos\left(\omega(\tau_l - \tau_k) + \phi_l - \phi_k\right) d\omega. \quad (23)$$

Note that $R^2(\omega) + I^2(\omega) = F_R^2(\omega)PN_R^2(\omega) + F_R^2(\omega)PN_I^2(\omega) = 2F_R^2(\omega)$, as both $PN_R(\omega)$ and $PN_I(\omega)$ are sequences of ± 1's, when no interference suppression is considered. Recalling that $f(t)$ is assumed to be even, it is important to observe that $(1/\pi)\int_{\omega_c-\pi W}^{\omega_c+\pi W} F_R^2(\omega)\cos(\omega(\tau_l - \tau_k))d\omega$ corresponds to the inverse Fourier transform of $F_R^2(\omega)$ evaluated at $t = \tau_l - \tau_k = (l-k)/W$. If the inverse Fourier transform of $F_R^2(\omega)$ is equal to zero for $l \ne k$, but is different from zero when $l = k$, the decision variable reduces to

$$\Delta = \left(\frac{1}{\pi}\int_{\omega_c-\pi W}^{\omega_c+\pi W}\left(R^2(\omega) + I^2(\omega)\right)d\omega\right)\sum_{l=0}^{L-1}\alpha_l^2 \quad (24)$$

when no interference suppression is used, and assuming MRC.

Observe that the term in brackets in the last equation is equal to the energy of the transmitted signal. A signal $f(t)$ with bandwidth W that is equal to zero for $t = k/W$, for any nonzero integer k, is $f(t) = W\mathrm{sinc}(Wt)$, where $\mathrm{sinc}(x) = \sin(\pi x)/(\pi x)$. Therefore, in this ideal case, there is no self-interference between the multipath components, independent of the spreading sequence used. In contrast, it is well known that in conventional spread-spectrum systems, the self-interference among the multipath components only goes to zero when the processing gain goes to infinity.

B. Time-Truncated Case

In this case, the information component of the decision variable is composed of a desired information component D and a self-interference component S. Therefore, we can rewrite (20) as

$$\Delta = D + S. \quad (25)$$

By substituting (13) and (14) in (20), the desired information component is given by

$$D = \frac{1}{\pi^2}\sum_{l=0}^{L-1}\alpha_l g_l \int_{-\frac{T}{2}}^{\frac{T}{2}}\left(\int_{\omega_c-\pi W}^{\omega_c+\pi W} R(\omega)\cos(\omega\xi - \phi_l) - I(\omega)\sin(\omega\xi - \phi_l)d\omega\right)^2 d\xi \quad (26)$$

and the self-interference component is given by

$$S = \frac{1}{\pi^2}\sum_{l=0}^{L-1}\sum_{\substack{k=0\\ l\ne k}}^{L-1}\alpha_l g_k \times \int_{-\frac{T}{2}}^{\frac{T}{2}}\left(\int_{\omega_c-\pi W}^{\omega_c+\pi W} R(\omega)\cos(\omega\xi - \phi_l) - I(\omega)\sin(\omega\xi - \phi_l)d\omega\right) \times \left(\int_{\omega_c-\pi W}^{\omega_c+\pi W} R(\omega)\cos\left(\omega(\xi - \tau_k + \tau_l) - \phi_k\right) - I(\omega)\sin\left(\omega(\xi - \tau_k + \tau_l) - \phi_k\right)d\omega\right)d\xi. \quad (27)$$

V. Noise and Interference Analysis

The noise and interference components in the decision variable are considered in this section. The noise $n_w(t)$ is modeled as a zero-mean additive white Gaussian process, with autocorrelation function equal to $R_n(\tau) = N_0/2\,\delta(\tau)$. The interference is modeled as a zero-mean wide-sense stationary (WSS) Gaussian process with PSD $S_I(\omega)$.

Since the receiver is linear, the information, noise, and interference can be treated separately. Denoting either the noise or the interference by $y(t)$, and assuming that $y(t)$ is the only signal at the receiver's input, the signal $y_1(t)$ at point 1 in Fig. 3 is obtained using a procedure similar to the one in Section IV, and is given by

$$y_1(t) \cong \frac{1}{2}\cos\left(\omega_a(t - t_0) + \beta_r(t - t_0)^2\right) \times \int_{-\frac{T}{2}}^{\frac{T}{2}+T_m} y(\xi + t_0)\cos\left(2\beta_r(t - t_0)\xi\right)d\xi + \frac{1}{2}\sin\left(\omega_a(t - t_0) + \beta_r(t - t_0)^2\right) \times \int_{-\frac{T}{2}}^{\frac{T}{2}+T_m} y(\xi + t_0)\sin\left(2\beta_r(t - t_0)\xi\right)d\xi. \quad (28)$$

After $y_1(t)$ passes through the RAKE receiver and LPF, $y_2(t)$ is generated and is equal to

$$\begin{aligned} y_2(t) = &\frac{2\beta_r}{\pi}\left(\int_{-\frac{T}{2}}^{\frac{T}{2}+T_m} y(\xi+t_0)\cos\left(2\beta_r(t-t_0)\xi\right)d\xi\right) \\ &\times \sum_{k=0}^{L-1} g_k \Lambda_c\left(2\beta_r(t-t_0),k\right) \\ &- \frac{2\beta_r}{\pi}\left(\int_{-\frac{T}{2}}^{\frac{T}{2}+T_m} y(\xi+t_0)\sin\left(2\beta_r(t-t_0)\xi\right)d\xi\right) \\ &\times \sum_{k=0}^{L-1} g_k \Lambda_s\left(2\beta_r(t-t_0),k\right) \end{aligned} \tag{29}$$

where $\Lambda_c(\omega,k)$ and $\Lambda_s(\omega,k)$ were defined in (17) and (18), respectively. Therefore, the component Y corresponding to $y(t)$ in the decision variable is obtained by integrating $y_2(t)$ over the frequency interval over which this function is valid, and is given by

$$\begin{aligned} Y = &\frac{1}{\pi}\sum_{k=0}^{L-1} g_k \int_{\omega_c-\pi W}^{\omega_c+\pi W}\int_{-\frac{T}{2}}^{\frac{T}{2}+T_m} y(\xi+t_0) \\ &\times\left(\cos(\omega\xi)\Lambda_c(\omega,k) - \sin(\omega\xi)\Lambda_s(\omega,k)\right)d\xi d\omega \end{aligned} \tag{30}$$

where the relation $\omega = 2\beta_r(t-t_0)$ is used.

A. Noise

Since the noise is Gaussian, the noise component of the decision variable is Gaussian, conditioned on the channel coefficients and phases. It can be seen from (30) that the mean value of the noise component is equal to zero, and its variance σ_n^2 is equal to

$$\begin{aligned} \sigma_n^2 = &\frac{N_0}{2\pi^2}\sum_{k=0}^{L-1}\sum_{k'=0}^{L-1} g_k g_{k'} \\ &\times\left[\int_{-\frac{T}{2}}^{\frac{T}{2}+T_m}\left(\int_{\omega_c-\pi W}^{\omega_c+\pi W} R(\omega)\cos\left(\omega(\xi-\tau_k)-\phi_k\right)\right.\right. \\ &\qquad\left. - I(\omega)\sin\left(\omega(\xi-\tau_k)-\phi_k\right)d\omega\right) \\ &\times\left(\int_{\omega_c-\pi W}^{\omega_c+\pi W} R(\omega)\cos\left(\omega(\xi-\tau_{k'})-\phi_{k'}\right)\right. \\ &\qquad\left.\left. - I(\omega)\sin\left(\omega(\xi-\tau_{k'})-\phi_{k'}\right)d\omega\right)d\xi\right]. \end{aligned} \tag{31}$$

Note in (31) that the noise components of different RAKE fingers are *correlated* (the noise-term variance is a function of $\sum_{k=0}^{L-1}\sum_{k'=0}^{L-1} g_k g_{k'}$, as opposed to the form $\sum_{k=0}^{L-1} g_k^2$).

The noise variance is obtained for the ideal Fourier transform case by letting $T\to\infty$ in the integral limits of (31). In this case, assuming MRC, σ_n^2 reduces to

$$\sigma_n^2 = \frac{N_0}{2}\left(\frac{1}{\pi}\int_{\omega_c-\pi W}^{\omega_c+\pi W}\left(R^2(\omega)+I^2(\omega)\right)d\omega\right)\sum_{k=0}^{L-1}\alpha_k^2 \tag{32}$$

where it is assumed that the inverse Fourier transform of $F_R^2(\omega)$ is equal to zero for $k\neq k'$, as discussed in Section IV. Note that in this ideal case, the noise components for different multipath components are independent. In a conventional DS/CDMA system, the noise components in different RAKE fingers are uncorrelated when the processing gain goes to infinity. It should be observed that the term in brackets in (32) is the transmitted signal energy. Therefore, it can be seen from (24) and (32) that this system functions as an ideal binary phase-shift keying (BPSK) system with MRC when the Fourier transform operates over all time.

B. Gaussian Interference

As in the additive white Gaussian noise (AWGN) case, it can be seen in (30) that conditioned on the channel coefficients and phases, the interference component is a zero-mean Gaussian variable with variance equal to

$$\begin{aligned} \sigma_I^2 = &\frac{1}{\pi^2}\sum_{k=0}^{L-1}\sum_{k'=0}^{L-1} g_k g_{k'} \\ &\times\left[\frac{1}{2\pi}\int_{-\infty}^{\infty} S_I(\beta)\right. \\ &\times\left(\int_{\omega_c-\pi W}^{\omega_c+\pi W}\int_{-\frac{T}{2}}^{\frac{T}{2}+T_m}\left(R(\omega)\cos(\omega(\xi-\tau_k)-\phi_k)\right.\right. \\ &\qquad\left.\left. - I(\omega)\sin(\omega(\xi-\tau_k)-\phi_k)\right)e^{j\beta\xi}d\xi d\omega\right) \\ &\times\left(\int_{\omega_c-\pi W}^{\omega_c+\pi W}\int_{-\frac{T}{2}}^{\frac{T}{2}+T_m}\left(R(\omega)\cos(\omega(\xi-\tau_{k'})-\phi_{k'})\right.\right. \\ &\qquad\left.\left.\left. - I(\omega)\sin(\omega(\xi-\tau_{k'})-\phi_{k'})\right)e^{-j\beta\xi}d\xi d\omega\right)d\beta\right]. \end{aligned} \tag{33}$$

Due to the finite observation time of the Fourier transform device, it is possible that NBI spectral leakage occurs.[4] To reduce this phenomenon, the following techniques could be used: time windowing, continuous processing, and increasing the excision bandwidth. Time windowing was considered in combination with the use of SAW devices in [33], assuming a spread-spectrum system. In this paper, we assume knowledge of the NBI frequency occupancy. Since the proposed system is frequency-domain based, spectral-encoded systems can more easily detect

[4]Recall that the time truncation of the Fourier transform device corresponds to the convolution of the desired spectrum by the Fourier transform of the time window. In our case, the time window is a rectangular function, which has a sinc-like spectrum. The sinc function has sidelobes that are relatively high, and decay very slowly. Therefore, when real-time Fourier transform devices are used, the PSD of the NBI leaks to adjacent frequencies.

the presence of NBI and estimate its frequency occupancy. For example, a received signal-strength indicator can be used.

When ideal Fourier transform devices are considered, σ_I^2 reduces to

$$\sigma_I^2 = \sum_{k=0}^{L-1}\sum_{k'=0}^{L-1} g_k g_{k'} \frac{1}{\pi} \int_{\omega_c-\pi W}^{\omega_c+\pi W} S_I(\omega)\left(R^2(\omega)+I^2(\omega)\right) \times \cos\left(\omega(\tau_k-\tau_{k'})+\phi_k-\phi_{k'}\right) d\omega. \quad (34)$$

In the derivations of (33) and (34), we used the spectral representation of random processes derived in [34, Sec. 11-4].

VI. Numerical Results

The conditional probability of error, assuming equally likely symbols, is given by

$$P_e\left|\{\alpha_l,\phi_l\}_{l=0}^{L-1} = \frac{1}{2}\operatorname{erfc}\left(\frac{D+S}{\sqrt{2\left(\sigma_n^2+\sigma_I^2\right)}}\right) \quad (35)$$

where D is the information component, S is the self-interference, σ_n^2 is the noise variance, and σ_I^2 is the Gaussian interference variance, given by (26), (27), (31), and (33), respectively, when a time-truncated Fourier transform device is used. When ideal Fourier transform devices are considered, the self-interference component S is zero, and D, σ_n^2, and σ_I^2 are given by (24), (32), and (34), respectively. It is important to note that the "RAKE fingers" in the proposed receiver are correlated, due to the Fourier transform time-truncation and to the presence of NBI. Therefore, (35) is a function of $\sum_{k=0}^{L-1}\sum_{k'=0}^{L-1} g_k g_{k'}$, instead of $\sum_{k=0}^{L-1} g_k^2$. This fact greatly increases the difficulty in obtaining a closed-form solution for the unconditional probability of error, and analyses such as the ones in [35] and [36], for example, do not directly apply.

It is seen in (27), (31), and (33) that the self-interference term, the correlation of the noise components, and the correlation of the NBI terms in the time-truncated Fourier transform case are a function of the time-truncation window T. This parameter should be made as large as possible, to minimize the previously mentioned effects, but is limited by Fourier transform real-time implementations, which are a function, among others, of the signal bandwidth. The performance of the proposed system as a function of the truncation window T is shown in Fig. 4. It is seen, as expected, that the shorter the truncation window, the worse the system performance. This is due to both the self-interference and the mismatch between the received signal and the receiver template. It can be seen that the system performance closely approaches that of a system using ideal Fourier transform devices for $T = 80$ ns. To reduce the effects of the time-truncated Fourier transformation, i.e., to reduce the self-interference component and the NBI spectral leakage, we use $T = 200$ ns in the numerical results that follow.

In this section, we assume two well-known UWB channel models. The first model to be considered [26] is a conventional tapped delay line, which allows for a theoretical analysis. In this case, the unconditional probability of error is obtained by averaging the conditional probability of error (35) over the joint probability density function (pdf) of the channel coefficients and phases. Due to the very large number of multipath coefficients,

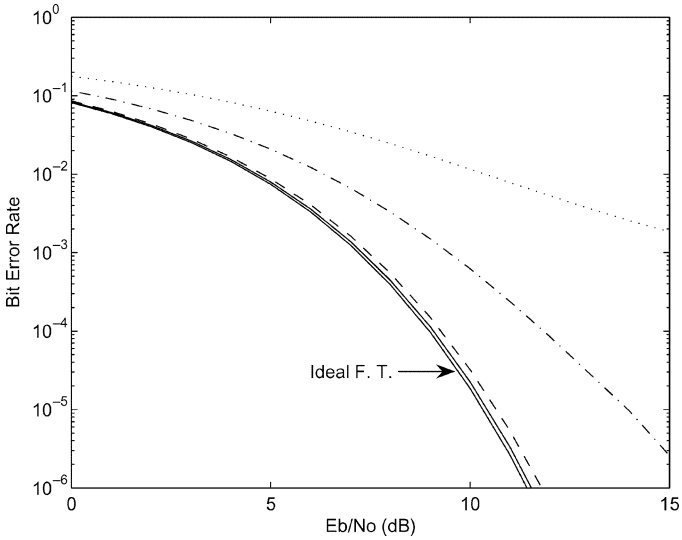

Fig. 4. BER for different observation intervals of the Fourier transform devices in the absence of NBI. The channel model presented in [26] is used. $T = 10$ (dotted line), 20 (dash-dot), 40 (dashed), and 80 ns (solid).

the complexity of this procedure can become prohibitive, and the averaging is performed by using Lepage's numerical integration algorithm [37]. In the channel model proposed in [26], the multipath coefficients are independent Nakagami variables, with random fading parameters and second moments. In the numerical results that follow, using an approach similar to the one taken in [38], these parameters are fixed to their mean values.

The second channel model to be considered is the one proposed by the IEEE 802.15 Channel Modeling subcommittee [28]. In this model, the multipaths are assumed to arrive in clusters, and the multipath amplitudes follow a lognormal fading distribution. Due to the complexity of this model, the unconditional probability is obtained via simulation by averaging the conditional probability of error over 10^7 different channel realizations. When using the IEEE model, we use a set of input parameters that corresponds to an LOS situation with range equal to 0–4 m [28].

The signal $f(t)$ is taken to be $f(t) = W\operatorname{sinc}(Wt)$, with $W = 500$ MHz. Therefore, for both channel models, it is assumed that a time resolution equal to 2 ns is achieved in the multipath delay profile. The transmitted signal occupies the range 3.1–3.6 GHz. The spreading sequence is considered to be purely real and given by $-1, -1, -1, -1, 1, 1, 1, -1, 1, 1, -1, -1, 1, -1, 1$, with each chip having bandwidth equal to 500 MHz/15 chips ≈ 33 MHz. The PSD $S_I(\omega)$ of the Gaussian interference is assumed to be given by

$$S_I(\omega) = \begin{cases} \frac{N_I}{2}, & \omega_c - \pi\mathrm{BW} \le |\omega| \le \omega_c + \pi\mathrm{BW} \\ 0, & \text{otherwise} \end{cases} \quad (36)$$

where the bandwidth BW is equal to 25 MHz, and centered around $f_c = 3.35$ GHz. When interference suppression is considered, the eighth chip is set to zero.

The system performance when the first channel model is used is shown in Fig. 5, assuming MRC. It is seen in this figure that the system performance is severely affected by the NBI when no suppression is used. It can also be observed that the system performance significantly improves when interference suppression is used independent of the SIR value. It should be noted that

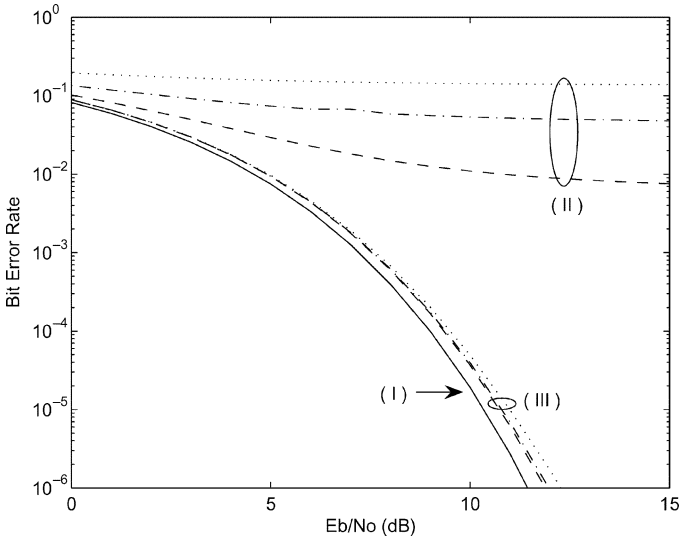

Fig. 5. BER assuming the channel model presented in [26] and MRC. (I) Absence of NBI. (II) No NBI suppression. (III) NBI suppression. SIR is equal to -5 (dashed lines), -10 (dash-dot), and -15 dB (dotted).

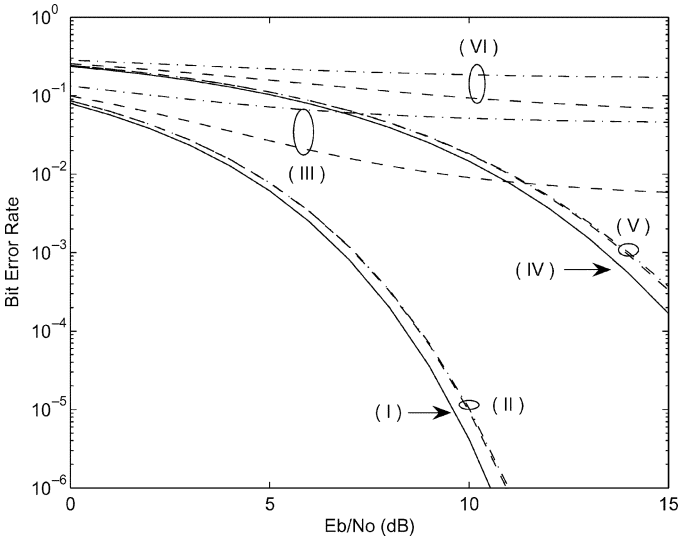

Fig. 6. BER assuming the IEEE channel model. (I) Absence of NBI (MRC). (II) NBI suppression (MRC). (III) No NBI suppression (MRC). (IV) Absence of NBI (EGC). (V) NBI suppression (EGC). (VI) No NBI suppression (EGC). SIR is equal to -10 (dashed lines) and -15 dB (dash-dot).

the small difference in performance for the three different SIR cases, when NBI suppression is used, is due to the NBI spectral leakage resulting from the Fourier transform's time truncation. It is also seen that there is a gap in the system performance when only thermal noise is present and when NBI suppression is used. This is expected, because when the suppression scheme notches out the frequency components where the interference is located, desired signal energy is also lost. To obtain the curve corresponding to ideal Fourier transform devices, we used the pdf of $\sum_{k=0}^{L-1} \alpha_k^2$ derived in [39].

Consider now the IEEE channel model. The system performance for this model, using either MRC or EGC reception considering the first 30 received multipath components, is shown in Fig. 6. It can be seen, for both combining techniques, that the NBI-suppression technique greatly improves the system performance, and, in this case, the system performance closely approximates that of no NBI being present. It is also seen that the difference in performance between MRC and EGC is significant. As previously observed in [40], for a Nakagami environment, the difference in performance between EGC and MRC increases with the increase in the order of diversity (in this case, the order of diversity is very high, 30). Also, the difference between EGC and MRC is more accentuated for an exponential multipath intense profile, which is assumed for both channel models under consideration, when compared with a uniform intensity profile.

The performances of the generalized selection-combining techniques are presented in Figs. 7–10. In Fig. 7, the performances of SC/MRC and SC/EGC are evaluated in the absence of NBI for different numbers of combined multipath components. It is seen that for the SC/MRC technique, the larger the number of multipaths combined, the better is the system performance. However, after a certain number of multipath components are combined, the system performance does not significantly improve. In this figure, the curve corresponding to MRC overlaps the curve corresponding to SC/MRC, in which only the strongest 20 paths are combined. For SC/EGC, however, an increase in the number of selected multipath

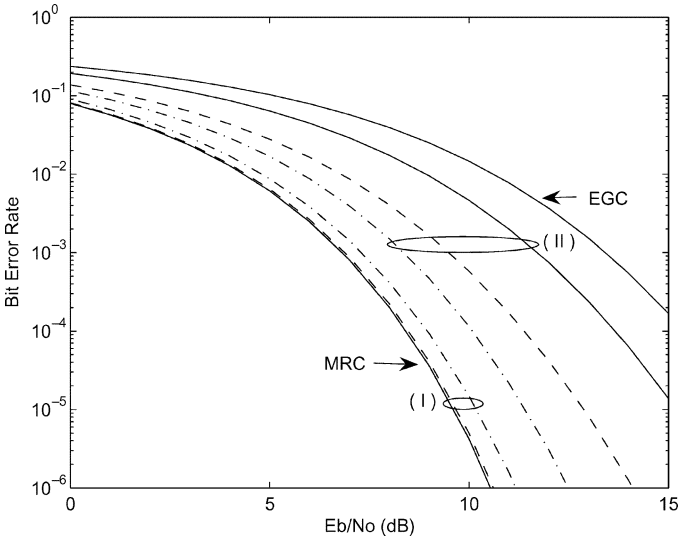

Fig. 7. BER assuming the IEEE channel model in the absence of NBI. (I) SC/MRC. (II) SC/EGC. Decision is made based on the 20 (solid lines), 10 (dashed), and 5 (dash-dot) components with largest absolute values, among the first 30 received multipath components.

components does not imply better performance. It is seen that the best performance is achieved when only five paths are combined. In a nonoptimum combining scheme such as EGC, the inclusion of the signal at one more finger may not be enough to counterbalance the addition of the noise present at that finger. In a UWB environment, where the multipath intensity profile is exponential, the addition of low-signal-power fingers can actually lead to a worse performance. This fact can be analytically seen in the BER expression for MRC and EGC, assuming orthogonal multipath components and a BPSK system. For MRC, the BER is given by $0.5\,\mathrm{erfc}\,(\sqrt{E_b/N_0}\cdot\sqrt{\alpha_0^2+\ldots+\alpha_{L-1}^2})$. It can be seen that the term $\sqrt{\alpha_0^2+\ldots+\alpha_{L-1}^2}$ always increases with the additional fingers. Consequently, the system performance always improves with the addition of more

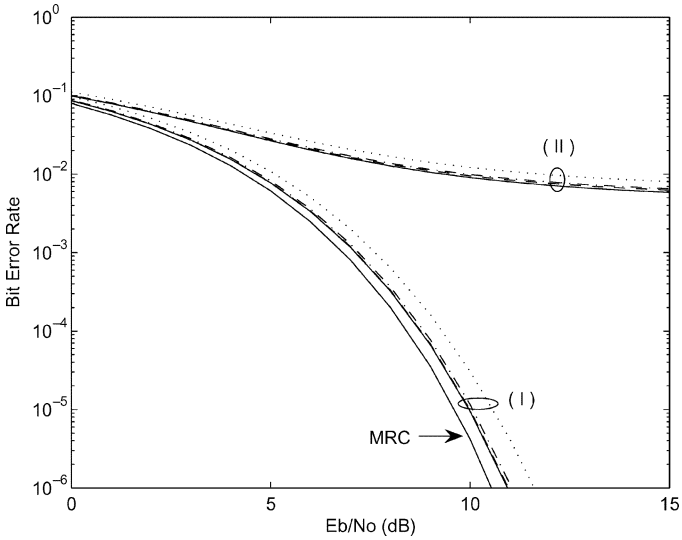

Fig. 8. BER assuming the IEEE channel model. SC/MRC. SIR $= -10$ dB. (I) NBI suppression. (II) No NBI suppression. Decision is made based on the 30 (solid lines), 20 (dashed), 10 (dash-dot), and 5 (dotted) multipath components with largest absolute values, among the first 30 received multipath components.

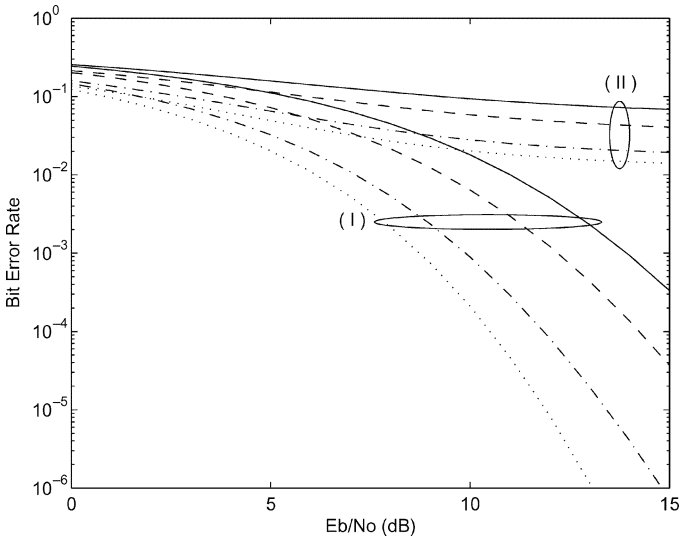

Fig. 9. BER assuming the IEEE channel model. SC/EGC. SIR $= -10$ dB. (I) NBI suppression. (II) No NBI suppression. Decision is made based on the 30 (solid lines), 20 (dashed), 10 (dash-dot), and 5 (dotted) multipath components with largest absolute values, among the first 30 received multipath components.

fingers. On the other hand, the BER expression for EGC is $0.5\,\mathrm{erfc}\,(\sqrt{E_b/N_0}\cdot(\alpha_0+\ldots+\alpha_{L-1}/\sqrt{L}))$. In this case, the increase in the numerator of the term $(\alpha_0+\ldots+\alpha_{L-1}/\sqrt{L})$ may not counterbalance the increase in the denominator if the signal power is too low. It should be noted that there is an analytical framework which provides the theoretical basis for deciding how many fingers should be included in the receiver [41], [42]. However, due to the complexity of the analysis of this system, the formulation presented in [41] and [42] could not be extended to the system developed here.

The performance of the generalized selection-combining techniques in the presence of NBI can be observed in Figs. 8 and 9. It can be seen that the performance of both SC/MRC and SC/EGC when NBI is present, both with and without NBI suppression, exhibits a similar behavior to when NBI is absent. For the SC/MRC technique, the larger the number of multipaths

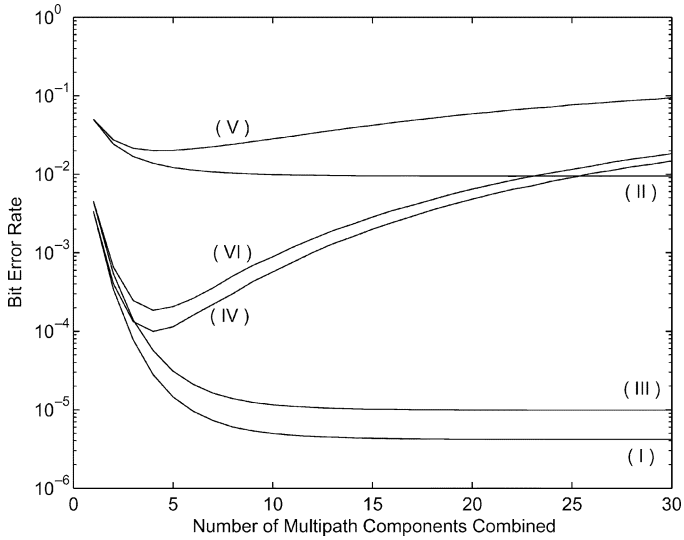

Fig. 10. BER assuming the IEEE channel model as a function of the number of multipath components combined. $E_b/N_0 = 10$ dB and SIR $= -10$ dB. (I) Absence of NBI (SC/MRC). (II) No NBI suppression (SC/MRC). (III) NBI suppression (SC/MRC). (IV) Absence of NBI (SC/EGC). (V) No NBI suppression (SC/EGC). (VI) NBI suppression (SC/EGC).

combined, the better is the system performance; while for the SC/EGC, when considering 5, 10, 20, or 30 paths, the best performance is achieved when only five multipath components are combined. The behavior of the generalized combining techniques as a function of the number of multipaths combined can be better observed in Fig. 10. As previously seen, the SC/MRC performance does not improve after a certain number of multipaths are combined. Also, it can be seen that there is an optimum number of multipath components that minimize the SC/EGC BER.

VII. Conclusion

The concept of spectral-encoded systems was extended in this paper to include NBI suppression via spectral shaping. The system performance was assessed by means of a theoretical analysis, and a detailed description of a possible implementation of this system using SAW devices was developed. It was shown that NBI can severely affect the performance of UWB systems, but a significant improvement in the system performance is obtained when the interference-suppression method described here is used. It was observed that the difference in performance between EGC and MRC is significant in a UWB environment, due to the large number of multipath components. Also, it was seen that the performance of SC/MRC does not improve after a certain number of multipath components are combined, and that there is an optimum number of multipath components that minimize the SC/EGC BER.

References

[1] Federal Commun. Commission, "Revision of part 15 of the commission's rules regarding ultra-wideband transmission,", ET-Docket 98-153, First Rep., Order, Apr. 2002.

[2] D. Porcino and W. Hirt, "Ultra-wideband radio technology: Potentials and challenges ahead," *IEEE Commun. Mag.*, vol. 41, pp. 66–74, Jul. 2003.

[3] M. Z. Win and R. A. Scholtz, "Impulse radio: How it works," *IEEE Commun. Lett.*, vol. 2, no. 2, pp. 36–38, Feb. 1998.

[4] M. Z. Win and R. A. Scholtz, "Ultra-wide bandwidth time-hopping spread-spectrum impulse radio for wireless multiple-access communications," *IEEE Trans. Commun.*, vol. 48, no. 4, pp. 679–691, Apr. 2000.
[5] K. Siwiak, "Ultra-wideband radio: Introducing a new technology," in *Proc. IEEE Veh. Technol. Conf.*, Rhodes, Greece, Spring 2001, pp. 1088–1093.
[6] M. Z. Win and R. A. Scholtz, "On the robustness of ultra-wide bandwidth signals in dense multipath environments," *IEEE Commun. Lett.*, vol. 2, no. 2, pp. 51–53, Feb. 1998.
[7] ——, "Characterization of ultra-wide bandwidth wireless indoor channels: A communication theoretic view," *IEEE J. Sel. Areas Commun.*, vol. 20, no. 12, pp. 1613–1627, Dec. 2002.
[8] S. Stroh, "Wideband: Multimedia unplugged," *IEEE Spectrum*, vol. 40, pp. 23–27, Sep. 2003.
[9] S. Roy, J. R. Foerster, V. S. Somayazulu, and D. G. Leeper, "Ultrawideband radio design: The promise of high-speed, short-range wireless connectivity," *Proc. IEEE*, vol. 92, no. 2, pp. 295–311, Feb. 2004.
[10] M. Welborn and M. Mc Laughlin, "Merger #2 Prop. DS-CDMA,", IEEE 802.15-03/334r1, Sep. 2003.
[11] A. Batra, "Multiband OFDM Physical Layer Proposal for IEEE 802.15 TG 3a,", IEEE 802.15-03/268r0, Jul. 2003.
[12] R. Fontana, A. Ameti, E. Richley, L. Beard, and D. Guy, "Recent advances in ultra wideband communications systems," in *Proc. IEEE Conf. Ultra-Wideband Syst. Technol.*, Baltimore, MD, 2002, pp. 129–133.
[13] M. Z. Win, X. Qiu, R. A. Scholtz, and V. O. K. Li, "ATM-based TH-SSMA network for multimedia PCS," *IEEE J. Sel. Areas Commun.*, vol. 17, no. 5, pp. 824–836, May 1999.
[14] Q. Li and L. A. Rusch, "Multiuser detection for DS-CDMA UWB in the home environment," *IEEE J. Sel. Areas Commun.*, vol. 20, no. 12, pp. 1701–1711, Dec. 2002.
[15] I. Bergel, E. Fishler, and H. Messer, "Narrowband interference suppression in time-hopping impulse-radio systems," in *Proc. IEEE Ultra-Wideband Syst. Technol.*, Baltimore, MD, 2002, pp. 303–307.
[16] D. Gerakoulis and P. Salmi, "An interference suppressing OFDM system for ultra-wide bandwidth radio channel," in *Proc. IEEE Ultra-Wideband Syst. Technol.*, Baltimore, MD, 2002, pp. 259–264.
[17] J. A. Salehi, A. M. Weiner, and J. P. Heritage, "Coherent ultrashort light pulse code-division multiple access communication systems," *J. Lightw. Technol.*, vol. 8, no. 3, pp. 478–491, Mar. 1990.
[18] K. S. Kim, D. M. Marom, L. B. Milstein, and Y. Fainman, "Hybrid pulse position modulation/ultrashort light pulse code-division multiple-access systems—Part I: Fundamental analysis," *IEEE Trans. Commun.*, vol. 50, no. 12, pp. 2018–2031, Dec. 2002.
[19] P. Crespo, M. L. Honig, and J. A. Salehi, "Spread-time code division multiple access," in *Proc. IEEE Globecom*, Phoenix, AZ, 1991, pp. 836–840.
[20] P. M. Crespo, M. L. Honig, and J. A. Salehi, "Spread-time code-division multiple access," *IEEE Trans. Commun.*, vol. 43, no. 6, pp. 2139–2148, Jun. 1995.
[21] M. G. Shayesteh, J. A. Salehi, and M. Nasiri-Kenari, "Spread-time CDMA resistance in fading channels," in *Proc. IEEE PIMRC*, San Diego, CA, 2001, pp. 115–119.
[22] ——, "Spread-time CDMA resistance in fading channels," *IEEE Trans. Wireless Commun.*, vol. 2, no. 3, pp. 446–458, May 2003.
[23] L. B. Milstein and P. K. Das, "An analysis of a real-time transform domain filtering digital communication system—Part I: Narrowband interference rejection," *IEEE Trans. Commun.*, vol. COM-28, no. 6, pp. 816–824, Jun. 1980.
[24] C. C. W. Ruppel, L. Reindl, and R. Weigel, "SAW devices and their wireless communications applications," *IEEE Microw. Mag.*, vol. 3, pp. 65–71, Jun. 2002.
[25] C. C. W. Ruppel and L. Reindl, "SAW devices for spread spectrum applications," in *Proc. IEEE Int. Symp. Spread-Spectrum Tech. Appl.*, Mainz, Germany, 1996, pp. 713–719.
[26] D. Cassioli, M. Z. Win, and A. F. Molisch, "The ultra-wide bandwidth indoor channel: From statistical models to simulation," *IEEE J. Sel. Areas Commun.*, vol. 20, no. 8, pp. 1247–1257, Aug. 2002.
[27] R. J. Cramer, R. A. Scholtz, and M. Z. Win, "Evaluation of an ultra-wide-band propagation channel," *IEEE Trans. Antennas Propag.*, vol. 50, no. 5, pp. 561–570, May 2002.
[28] IEEE P802.15 Working Group, "Channel Modeling Subcommittee Rep. Final,", IEEE P802.15/368r5-SG3a.
[29] J. G. Proakis, *Digital Communications*, 2nd ed. New York: McGraw-Hill, 1989.
[30] M. Z. Win and R. A. Scholtz, "On the energy capture of ultrawide bandwidth signals in dense multipath environments," *IEEE Commun. Lett.*, vol. 2, no. 9, pp. 245–247, Sep. 1998.
[31] T. Eng, N. Kong, and L. B. Milstein, "Comparison of diversity combining techniques for Rayleigh-fading channels," *IEEE Trans. Commun.*, vol. 44, no. 9, pp. 1117–1129, Sep. 1996.
[32] C. R. C. M. da Silva, "Performance of spectral-encoded ultra-wideband communication systems in the presence of narrow-band interference," Ph.D. dissertation, Univ. Calif. San Diego, La Jolla, CA, 2005.
[33] J. Gevargiz, P. K. Das, and L. B. Milstein, "Adaptive narrow-band interference rejection in a DS spread-spectrum intercept receiver using transform domain signal processing techniques," *IEEE Trans. Commun.*, vol. 37, no. 12, pp. 1359–1366, Dec. 1989.
[34] A. Papoulis and S. U. Pillai, *Probability, Random Variables and Stochastic Processes*, 4th ed. New York: McGraw-Hill, 2002.
[35] M. Z. Win and Z. A. Kostic, "Virtual path analysis of selective RAKE receiver in dense multipath channels," *IEEE Commun. Lett.*, vol. 3, no. 11, pp. 308–310, Nov. 1999.
[36] M. K. Simon and M.-S. Alouini, "A unified approach to the performance analysis of digital communication over generalized fading channels," *Proc. IEEE*, vol. 86, no. 9, pp. 1860–1877, Sep. 1998.
[37] G. Lepage, "A new algorithm for adaptive multidimensional integration," *J. Computat. Phys.*, vol. 27, pp. 192–203, 1978.
[38] D. Cassioli, M. Z. Win, F. Vatalaro, and A. F. Molisch, "Performance of low-complexity RAKE reception in a realistic UWB channel," in *Proc. IEEE ICC*, New York, NY, 2002, pp. 763–767.
[39] M.-S. Alouini, A. Abdi, and M. Kaveh, "Sum of gamma variates and performance of wireless communication systems over Nakagami-fading channels," *IEEE Trans. Veh. Technol.*, vol. 50, no. 6, pp. 1471–1480, Nov. 2001.
[40] M.-S. Alouini and M. K. Simon, "Performance analysis of coherent equal gain combining over Nakagami-m fading channels," *IEEE Trans. Veh. Technol.*, vol. 50, no. 6, pp. 1449–1463, Nov. 2001.
[41] M. Z. Win, G. Chrisikos, and N. R. Sollenberger, "Effects of chip rate on selective RAKE combining," *IEEE Commun. Lett.*, vol. 4, no. 7, pp. 233–235, Jul. 2000.
[42] ——, "Performance of RAKE reception in dense multipath channels: Implications of spreading bandwidth and selection diversity order," *IEEE J. Sel. Areas Commun.*, vol. 18, no. 8, pp. 1516–1525, Aug. 2000.

Claudio R. C. M. da Silva (S'99) received the B.S. and M.Sc. degrees in electrical engineering from the State University of Campinas (UNICAMP), Campinas, Brazil, in 1999 and 2001, respectively. Since 2001, he has been working toward the Ph.D. degree at the University of California at San Diego, La Jolla, in the area of communication theory and systems.

Mr. da Silva was awarded a fellowship from the California Institute of Telecommunications and Information Technology for the academic year 2001–2002. He received the 2003 IEEE Conference on Ultra-Wideband Systems and Technologies Student Paper Prize.

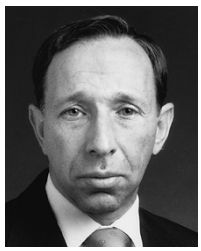

Laurence B. Milstein (S'66–M'68–SM'77–F'85) received the B.E.E. degree from the City College of New York, New York, NY, in 1964, and the M.S. and Ph.D. degrees in electrical engineering from the Polytechnic Institute of Brooklyn, Brooklyn, NY, in 1966 and 1968, respectively.

From 1968 to 1974, he was with the Space and Communications Group of Hughes Aircraft Company, and from 1974 to 1976, he was a member of the Department of Electrical and Systems Engineering, Rensselaer Polytechnic Institute, Troy, NY. Since 1976, he has been with the Department of Electrical and Computer Engineering, University of California at San Diego, La Jolla, where he is a Professor and former Department Chairman, working in the area of digital communication theory with special emphasis on spread-spectrum communication systems. He has also been a consultant to both government and industry in the areas of radar and communications.

Dr. Milstein was an Associate Editor for Communication Theory for the IEEE TRANSACTIONS ON COMMUNICATIONS, an Associate Editor for Book Reviews for the IEEE TRANSACTIONS ON INFORMATION THEORY, an Associate Technical Editor for the *IEEE Communications Magazine*, and the Editor-in-Chief of the IEEE JOURNAL ON SELECTED AREAS IN COMMUNICATIONS. He was the Vice President for Technical Affairs in 1990 and 1991 of the IEEE Communications Society, and has been a member of the Board of Governors of both the IEEE Communications Society and the IEEE Information Theory Society. He is a former Chair of the IEEE Fellows Selection Committee, and a former Chair of ComSoc's Strategic Planning Committee. He is a recipient of the 1998 Military Communications Conference Long Term Technical Achievement Award, an Academic Senate 1999 UCSD Distinguished Teaching Award, an IEEE Third Millenium Medal in 2000, the 2000 IEEE Communication Society Armstrong Technical Achievement Award, and the 2002 MILCOM Fred Ellersick Award.